Since January 2020 Elsevier has created a COVID-19 resource centre with free information in English and Mandarin on the novel coronavirus COVID-19. The COVID-19 resource centre is hosted on Elsevier Connect, the company's public news and information website.

The Journal of Supercritical Fluids 186 (2022) 105604

Contents lists available at ScienceDirect

The Journal of Supercritical Fluids

journal homepage: www.elsevier.com/locate/supflu

Production of carrier/antioxidant particles by Supercritical Assisted Atomization as an adjuvant treatment of the CoVID-19 pathology

Iolanda De Marco [a,b]

[a] Department of Industrial Engineering, University of Salerno, Via Giovanni Paolo II, 132, 84084 Fisciano, SA, Italy
[b] Research Centre for Biomaterials BIONAM, University of Salerno, Via Giovanni Paolo II, 132, 84084 Fisciano, SA, Italy

HIGHLIGHTS

- SAA process to obtain inclusion complexes and coprecipitated powders.
- HP-β-CD/API particles with a mean diameter equal to 0.46–0.69 μm were obtained.
- PVP/API powder in the range 0.40–0.45 μm were obtained.
- The dissolution rate of the SAA processed powders was speeded for all the flavonoids.

GRAPHICAL ABSTRACT

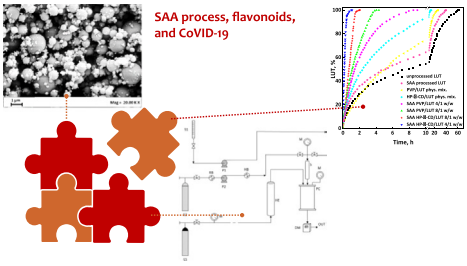

ARTICLE INFO

Keywords:
SAA coprecipitation
Bioavailability
Supercritical carbon dioxide
Micrometric particles

ABSTRACT

The 2019 coronavirus outbreak caused a global health emergency. Some therapeutic strategies for this pathology focus on natural compounds, such as flavonoids, because of their antimicrobial and antiviral properties. However, the therapeutic efficacy of these active compounds is limited by their low bioavailability. In this paper, composite systems consisting of the flavonoid and a carrier were produced by Supercritical Assisted Atomization to increase these compounds' dissolution rate. Luteolin, rutin, and naringenin were selected as model flavonoids, and hydroxypropyl-β-cyclodextrin and polyvinylpyrrolidone were chosen as the carriers. Hydroxypropyl-β-cyclodextrin was the most suitable carrier, in terms of recovery, morphology/size of the particles, and dissolution rate of the active compound. At the best operating conditions, the dissolution rate of the active principle is speeded for all the flavonoids: in particular, if compared to the virgin materials, it is 55.8 times faster for luteolin, 3.1 times faster for rutin and 3.4 times faster for naringenin.

1. Introduction

CoVID-19 (Corona Virus Disease 2019) is an acute respiratory disease caused by SARS-CoV-2, a new coronavirus that first appeared at the end of 2019 in Wuhan, China. Compared to other coronaviruses, it shows faster human-to-human transmission [1], which has led to immediate spread globally, alerting the World Health Organization (WHO), which declared a pandemic on 11 March 2020. Although more than one year has passed, the world is still looking for an effective therapeutic strategy to combat the epidemic; as new drugs could take a few months or even years, those already valid for other diseases are currently being used. Up to now, patients have been treated with viral agents, including oseltamivir [2], lopinavir/ritonavir tablets [3], remdesivir [4], and ribavirin (in combination with corticosteroids and/or interferon) [5,6]. Although the effectiveness of these drugs is still being evaluated, some severe side effects are a cause for concern, such as

E-mail address: idemarco@unisa.it.

https://doi.org/10.1016/j.supflu.2022.105604
Received 4 January 2022; Received in revised form 27 February 2022; Accepted 6 April 2022
Available online 9 April 2022

adverse hematological toxicity, arrhythmias, or hypotensive effects [7–9].

This underlines the urgency of therapeutic approaches that are effective but also safe. Natural products could be a significant resource with these premises as they have fewer side effects than synthetic drugs. Over the years, there has been a growing interest in using natural compounds, such as flavonoids, which bring numerous benefits to human health. Indeed, their efficacy has been demonstrated against cardiovascular and degenerative diseases; flavonoids have also been used for their antioxidant, antibacterial, hepatoprotective, anti-inflammatory, antitumor, and antiviral effects [10–12]. Antioxidant compounds have also shown a significant role in treating respiratory diseases, an essential requirement for a drug to be effective against CoVID-19 [12].

Filippini et al. [13] and Tutunchi et al. [14] suggest naringenin as a potential active principle against CoVID-19. Abd El-Aziz et al. [15] observed that it could inhibit the enzymatic activity of RNA polymerase and thus prevent the replication of Sars-CoV-2. Traditional Chinese medicine has recommended using luteolin to treat infections caused by SARS-CoV-2 [16], while Patil et al. [12] confirmed the potential of rutin in inhibiting the crucial viral proteins SARS-CoV-2.

Despite the promising in vitro results, one of the main limitations of flavonoids in "in vivo" studies is their poor solubility in water and, consequently, their low bioavailability, which implies the use of high dosages to obtain a therapeutic concentration in plasma [8,17]. To cope with this problem, micronization techniques can be exploited, making it possible to reduce the size of the active principle particles; in this way, the surface area exposed in contact with the dissolution medium increases and, therefore, also its dissolution speed. Another possible way to improve the bioavailability of hydrophobic compounds is their coprecipitation with hydrophilic carriers [18,19].

Among the various coprecipitation techniques, the processes based on the use of supercritical carbon dioxide ($scCO_2$) represent a valid alternative to conventional approaches since they allow to obtain a reasonable control of the powders' morphology and the particle size distribution, avoiding degradation phenomena or product contamination [20–23]. Indeed, $scCO_2$ has low critical temperature and pressure values and properties intermediate between the ones of liquids and gases [24]. If the carrier chosen for the coprecipitation through $scCO_2$ is a water-soluble polymer, it is possible to obtain a speeding up of the dissolution of the active pharmaceutical ingredient (API) and a consequent increase in its bioavailability [19,25,26].

Supercritical assisted atomization (SAA) has been frequently and efficiently used to obtain coprecipitated microparticles constituted by a carrier (which can be polymeric or not) in which the API is uniformly dispersed [27–29].

From an analysis of the literature, it appears that flavonoids have rarely been processed through the SAA process. In particular, luteolin was coprecipitated with dextran [18] or with polyvinylpyrrolidone (PVP) [30].

The choice of the polymeric carrier is fundamental because some polymers, such as PVP [31], are suitable when the dissolution of the active ingredient has to be speeded up; others, such as zein [32], delay the release and, therefore, can be used when a controlled or a prolonged release is desired. The processing with cyclodextrins, natural cyclic oligosaccharides with a three-dimensional structure that forces the hydroxyl groups on the outer edges, is fascinating. At the same time, in the cavity, there are only hydrogen atoms and oxygen bridges. It means that the central cavity has a hydrophobic nature, while the outer part is hydrophilic: this results in the possibility for the cyclodextrins to host hydrophobic molecules inside the cavity and be soluble in water. When a molecule of suitable polarity and size is housed in the cyclodextrin cavity, a so-called inclusion complex is formed [33].

In this paper, the effect of the polymeric carrier on the SAA coprecipitation of three different flavonoids: luteolin (LUT), rutin (RUT), and naringenin (NAR) was studied, to obtain powders with a rapid release of the API. The three active principles were SAA processed using PVP and hydroxypropyl-β-cyclodextrin (HP-β-CD) as the carriers to compare the coprecipitated powders (with PVP) and the inclusion complexes (with HP-β-CD) in terms of morphology, dimensions, and dissolution rates.

2. Materials and methods

2.1. Materials

Polyvinylpyrrolidone (PVP, average molecular weight of 10 kg/mol), hydroxypropyl-β-cyclodextrin (HP-β-CD, cavity diameter 0.60 nm and cavity height 0.78 nm, purity of 99.9%), rutin (RUT, $C_{27}H_{30}O_{16}$, molecular weight of 610.5 g/mol, purity of 95%), and naringenin (NAR, $C_{15}H_{12}O_5$, molecular weight of 272.3 g/mol, purity of 95%) were provided by Sigma–Aldrich (Milan, Italy); ethanol (EtOH, purity, 99.9%) was purchased from Carlo Erba Reagents (Cornaredo, Italy); luteolin (LUT, $C_{15}H_{10}O_6$, molecular weight of 286.2 g/mol, purity of 97%) was kindly supplied by Epitech Group (Milan, Italy). Carbon dioxide (CO_2, purity 99%) was provided by Morlando Group s.r.l. (Sant'Antimo, Naples, Italy), and nitrogen (N_2, purity 99.9%) by SOL (Naples, Italy).

Chemical structures of PVP monomer, HP-β-CD, RUT, LUT, and NAR are reported in Fig. 1.

The active principles' and carriers' solubilities in the solvents used for the experimentation were measured under ambient conditions and are reported in Table 1.

2.2. SAA apparatus and procedure

The homemade bench-scale SAA apparatus is sketched in Fig. 2.

Briefly, the CO_2 (stored in tank S2) is cooled in a refrigerating bath RB and then pumped by P2; carbon dioxide is pre-heated in HB, before reaching the saturator S, which is a high-pressure vessel (25 cm^3 internal volume). In the saturator, 5 mm perforated Berl saddles are placed to favor optimal contact between the liquid phase and the supercritical phase and allow the thermodynamic equilibrium achievement. Another high-pressure pump (P1) is used for the liquid solution (stored in the buret S1), which is contituted by the solutes (1 g for each test) dissolved in 100 mL of liquid solvent. Carbon dioxide dissolves in the liquid solution, and the mixture formed is sprayed from the saturator S to the atmospheric-pressure precipitation chamber PC (3000 cm^3 internal volume) through an 80 μm internal-diameter stainless-steel nozzle. Nitrogen stored in a tank (S3) and heated in an electric heat exchanger (HE) enters in a controlled manner (1200 nL/h) from the top of the precipitation vessel and assured the liquid droplets' evaporation. The temperature control is ensured by controllers connected with electrically thin bands, whereas the pressure is determined by a test gauge manometer (M). The precipitated powder is collected at the bottom of the precipitation chamber on a stainless-steel filter (size of pores of around 0.1 μm). The total quantity of delivered CO_2 is measured at the exit by a dry test meter (DM). Micronization experiments were performed in triplicates.

2.3. Characterization

Field-emission scanning electron microscopy (FESEM) was used to observe the morphology of the powders, after their covering with a thin layer of gold-palladium by sputtering. Images were acquired using a Carl Zeiss microscope (model LEO 1525, Carl Zeiss SMT AG, Oberkochen, Germany). Starting from high-magnification FESEM images, the Sigma Scan Pro image analysis software (version 5.0, Aspire Software International Ashburn, VA, USA) and the Microcal Origin software (version 8.0, Northampton, MA, USA) were used to measure the diameter of the particles and evaluate the powder particle size distribution (PSD).

Fourier-transform infrared (FTIR) analysis was carried out using a Bruker spectrophotometer (Bruker Optics, Ettlingen, Germany), model Vortex 70 FT-IR (scan wavenumber range of 4000–450 cm^{-1}, resolution

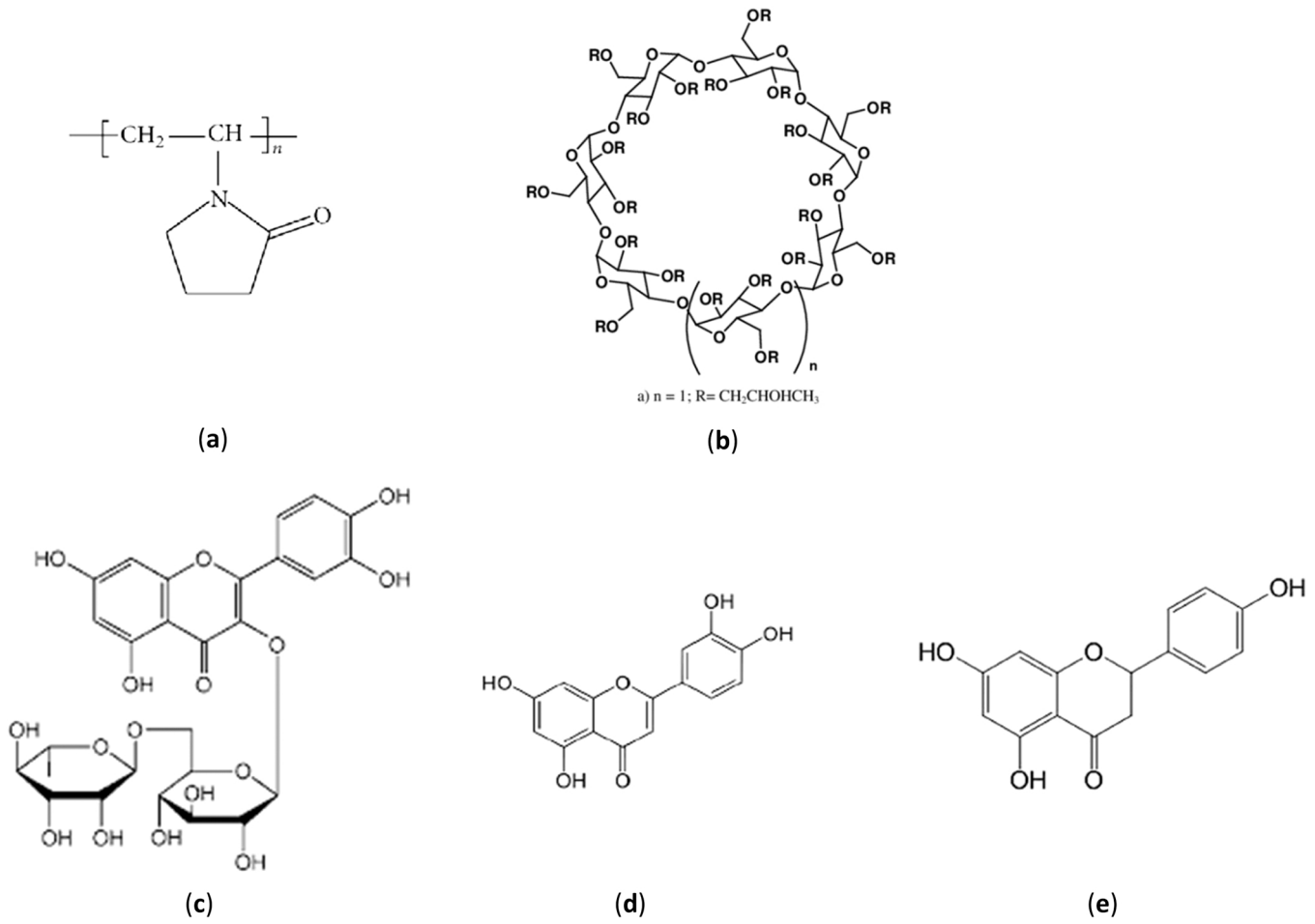

Fig. 1. Chemical structures of the involved materials: (a) PVP monomer; (b) HP-β-cyclodextrin; (c) rutin; (d) luteolin; (e) naringenin.

Table 1
Solubility of LUT, RUT, NAR, PVP, and HP-β-CD in pure ethanol and ethanol/water mixtures.

Solute	Solvent (*v*/*v*)	Solubility (mg/mL)
LUT	EtOH	5
	EtOH/H_2O 70/30	5
RUT	EtOH	20
	EtOH/H_2O 70/30	10
NAR	EtOH	2.5
	EtOH/H_2O 70/30	2
PVP	EtOH	200
HP-β-CD	EtOH/H_2O 70/30	120

of 0.5 cm^{-1} as the mean of 16 measurements).

Differential scanning calorimetry (DSC, mod. TC11, Mettler-Toledo, Inc., Columbus, OH, USA) was used to evaluate the thermal characteristics of the powders. A weithed amount of the powder (5 ± 0.5 mg) was heated from 30 °C up to 350 °C (with a scanning rate of 10 °C/min) using a nitrogen gas flow equal to 50 mL/min.

X-ray diffraction (XRD) analyses were performed using an X-ray powder diffractometer (model D8 Discover; Bruker, MA, USA). Powders were placed on a holder and flattened with a glass slide to minimize preferred orientation of the particles. XRD patterns were recorded using the following conditions: Ni-filtered CuKα radiation, λ = 1.54 Å, 2θ angle ranging from 10° to 50° with a step size of 0.03° and a scan rate of 0.2 s/step.

The loading of the active ingredient into the carrier was measured using a UV/vis spectrophotometer (Cary 50, Varian, Palo Alto, CA, USA) at the wavelength characteristic of the flavonoid (275 nm for LUT, 257 nm for RUT, and 288 nm for NAR) was detected. A fixed amount of the sample was dissolved in ethanol (2 mg of LUT in 50 mL_{EtOH}, 5 mg of RUT in 40 mL_{EtOH}, and 1 mg of NAR in 10 mL_{EtOH}) and analyzed to determine the drug concentration in the samples and estimate the yield, which is defined as the actual measured API content and the theoretical one ratio. For the preparation of the blank test, a weight amount of the carrier (5 mg) was dissolved in ethanol, and the value of the absorbance of the blank test was subtracted to the sample absorbance, to minimize the effect of the presence of the carrier on the results.

Dissolution tests were performed using the identical UV/vis spectrophotometer in the following conditions: in the case of LUT and RUT, phosphate-buffered saline (PBS) at pH 7.4 was used as the liquid medium, which simulates colon environment, in agreement with the literature [18,34], whereas, in the case of NAR, PBS at 6.8 was prepared, to simulate the intestinal condition [35]. Calibration curves were evaluated using diluted standards at five different concentrations of the active principle in PBS to convert the absorbance into concentration. After the calibrations, samples to be analyzed were placed into a dialysis sack (cut-off of 12–14,000 Da) and suspended in 3 mL of PBS; the equivalent amount of API contained in the samples was 2 mg for LUT and 5 mg for RUT and NAR. Then, the sack containing the sample and the PBS was incubated inside a vessel containing 300 mL of PBS (pH=7.4) for LUT and RUT, and 300 mL of PBS (pH=6.8) for NAR; the medium was continuously stirred at 150 rpm and heated at 37 ± 0.5 °C (to simulate the body environment). Each analysis was interrupted when the plateau was reached, and all the API was released to the outer phase. Analyses were performed in triplicate, and the shown profiles are the average of the calculations.

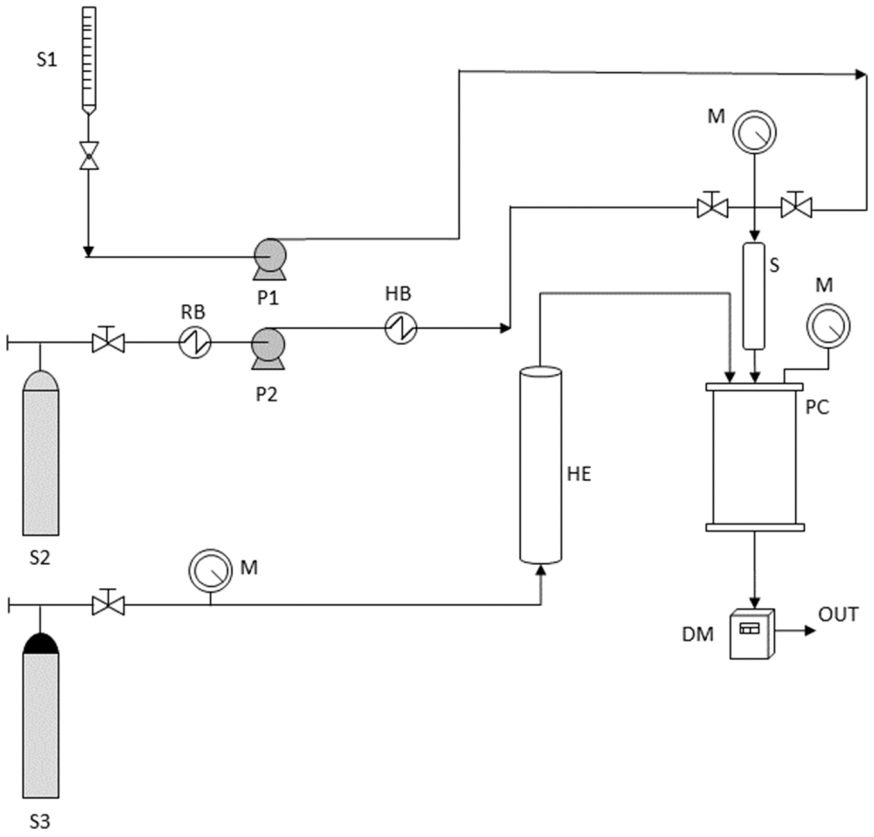

Fig. 2. A sketch of the SAA laboratory plant. S1, S2, and S3: liquid solution, carbon dioxide, and nitrogen vessels; P1 and P2: pumps; HB: heating bath; RB: refrigerating bath; HE: heat exchanger; M: manometer; S: high-pressure saturator; PC: precipitator; DM: dry test meter.

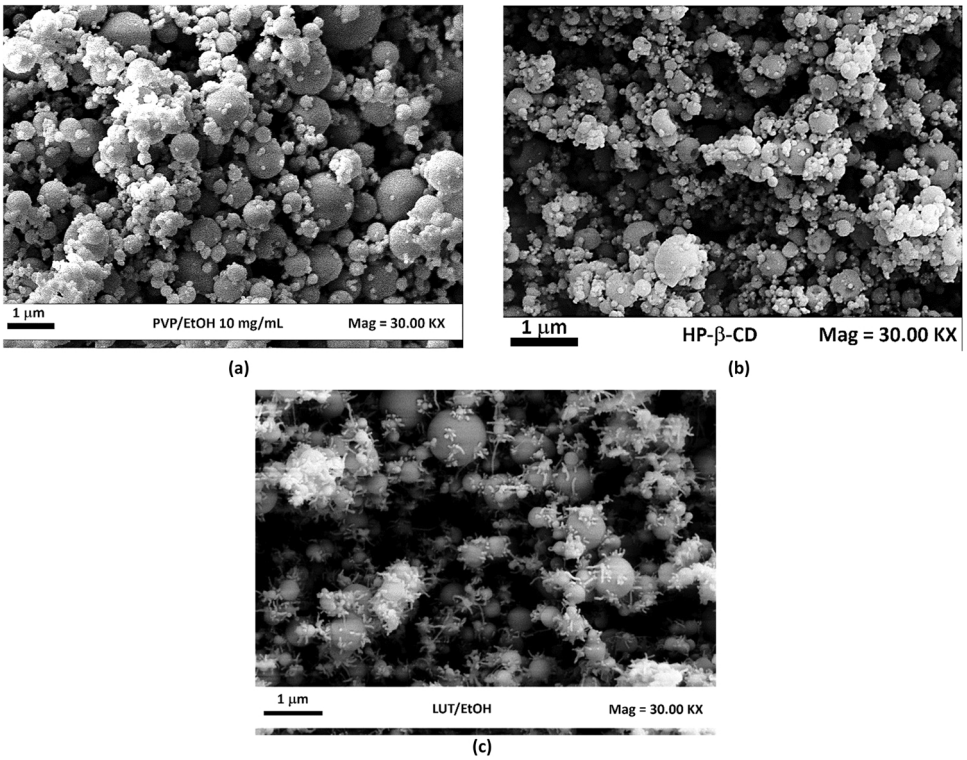

Fig. 3. FESEM images of pure compounds produced by SAA: (a) PVP; (b) HP-β-CD; (c) LUT.

3. Results and discussion

Some operating conditions have been fixed, considering that they have been optimized in previous studies [27,30]; for PVP, both the temperatures in the saturator and in the precipitation vessel were fixed at 80 °C, whereas the pressure was set at 9.0 MPa; for HP-β-CD, the temperature and the pressure in the saturator were fixed at 80 °C and 9.0 MPa, and the temperature in the precipitation chamber at 90 °C. According to previous literature studies, for both the carriers, the CO_2 flow rate was set at 5.4 g/min, and the solvent flow rate at 3 g/min to obtain a GLR (gas-to-liquid ratio) equal to 1.8, which is an optimal value for SAA micronization [27]. Before carrying out the coprecipitation experiments, the pure compounds were processed to underline the importance of using a carrier. The experiments revealed that PVP and HP-β-CD precipitated in form of well defined particles, as can be seen from the FESEM images reported in Figs. 3a and 3b. When pure antioxidants were processed, different results were observed: LUT particles tend to be spherical but it is possible to observe needles that indicate the beginning of a crystallization process (see the FESEM image in Fig. 3c); in the case of RUT and NAR, no powder was found in the SAA precipitator at the end of the experiments.

The coprecipitation experiments were carried out by varying the total concentration of the solutes in the liquid solution and the carrier/API ratio (*w/w*). The weight concentrations were chosen in order to obtain a HP-β-CD/API molar ratio equal to 2/1 and 1/1 that correspond to a 8/1 and 4/1 *w/w* ratio for LUT and RUT and to 9/1 and 4.5/1 *w/w* ratio for NAR.

When the coprecipitation was attempted with HP-β-CD as the carrier, EtOH/H_2O 70/30 *v/v* was used as the solvent; for the tests with PVP, the solution was prepared using ethanol. The chosen operating conditions are reported in Table 2, together with the observed morphology, the mean diameter (m.d.), the standard deviation (s.d.), and the yield of the produced particles.

3.1. Luteolin

The first active ingredient processed was LUT. In previous studies, the micronization of the compound alone had been attempted by the SAA process [18]; at the end of the experiments, a powder consisting of large crystals was obtained, whose dissolution rate was equal to that of the non-micronized compound. For this reason, it is central to assess whether the presence of a carrier can modify the bioavailability of the active ingredient. The SAA processing of LUT was then evaluated using first HP-β-CD and then PVP.

3.1.1. HP-β-CD/Luteolin

The first coprecipitation experiments (#1–3) were performed to evaluate the effect of the total concentration on the morphology, size, and particle size distribution (PSD) of the obtained particles, setting an HP-β-CD/Luteolin *w/w* ratio at 8/1 and varying the total concentration of the liquid solution from 10 to 30 mg/mL. In correspondence of all the tested operating concentrations, as evident from the FESEM images reported in Figs. 4a, 4b, and 4c, well-defined and regular sub-microparticles were precipitated. No luteolin crystals are noticeable, demonstrating that the presence of the carrier has controlled the recrystallization of the active principle and, therefore, improved LUT processability. The effect of the total concentration on the particle size and PSD is reported in Fig. 4d, which compares the cumulative volumetric distributions obtained for the processed particles. From this comparison, it is possible to observe a notable increase in the average diameter of the particles and in the standard deviation, passing from 10 mg/mL to 20 mg/mL. This behavior has been frequently observed using the SAA process; indeed, as the solute concentration increases, the viscosity of the solution rises, and larger droplets are formed at the outlet of the injector, resulting in the attainment of larger particles [18]. By further increasing the total concentration of the liquid solution (at 30 mg/mL), no noticeable variations in the particle size can be observed. However, particles are more collapsed (see Fig. 4c). For this reason, the latter concentration was not selected for the next set of experiments, performed varying the HP-β-CD/LUT ratio.

The effect of the HP-β-CD/LUT ratio on the morphology and size of the coprecipitated powders was subsequently evaluated to increase the relative amount of the flavonoid with respect to the carrier in composite powders. In particular, fixing the total concentration at 20 mg/mL, a lower carrier/API ratio, equal to 4/1 *w/w*, was evaluated. Also in this case, spherical particles with an average diameter of 0.69 μm were obtained. By comparing the cumulative volumetric distributions as the carrier/API ratio varies (test #2 and #4), it is observed that these are almost entirely superimposable; it can therefore be concluded that this parameter does not have a countless influence on the morphology and the mean size of the HP-β-CD/LUT particles.

3.1.2. PVP/Luteolin

To improve the processability and bioavailability of luteolin, this active principle was also coprecipitated with PVP, a hydrophilic polymer known for its ability to enhance the dissolution of hydrophobic drugs and avoid their recrystallization during the micronization process [19]. The total concentration was fixed at 10 mg/mL, a value optimized in previous works in which PVP was used as the carrier [30]. Two tests were carried out by varying the PVP/LUT ratio. The first test was performed at a polymer/API ratio equal to 8/1 *w/w*. In this case, the powders are collapsed, as shown from Fig. 5a; nevertheless, it was possible to determine the PSD of the particles that had a mean diameter equal to 0.45 μm. When the PVP/LUT ratio was decreased at 4/1 *w/w*, even more collapsed particles were obtained, for which it was not possible to determine the PSD. The morphological aspect of the powders

Table 2
SAA experiments conducted. aSMP: aggregated sub-microparticles; C_{tot}: total concentration of solutes; SMP: sub-microparticles; m.d.: mean diameter; s.d.: standard deviation.

#	API	Carrier	Carrier/API (*w/w*)	C_{tot} (mg/mL)	Morphology	m.d. ± s.d. [μm]	Yield%
1	LUT	HP-β-CD	8/1	10	SMP	0.41 ± 0.13	99.6
2				20	SMP	0.69 ± 0.22	100
3				30	aSMP	0.64 ± 0.19	99.9
4			4/1	20	SMP	0.69 ± 0.21	100
5		PVP	8/1	10	aSMP	0.45 ± 0.14	100
6			4/1		aSMP	–	99.9
7	RUT	HP-β-CD	4/1	10	SMP	0.42 ± 0.12	99.9
8				20	SMP	0.46 ± 0.13	100
9		PVP		10	No powder	–	–
10	NAR	HP-β-CD	9/1	20	SMP	0.57 ± 0.16	100
11			4.5/1	10	SMP	0.56 ± 0.30	99.9
12				20	SMP	0.63 ± 0.35	100
13				30	aSMP	0.83 ± 0.44	97
14		PVP	9/1	10	SMP	0.40 ± 0.12	100

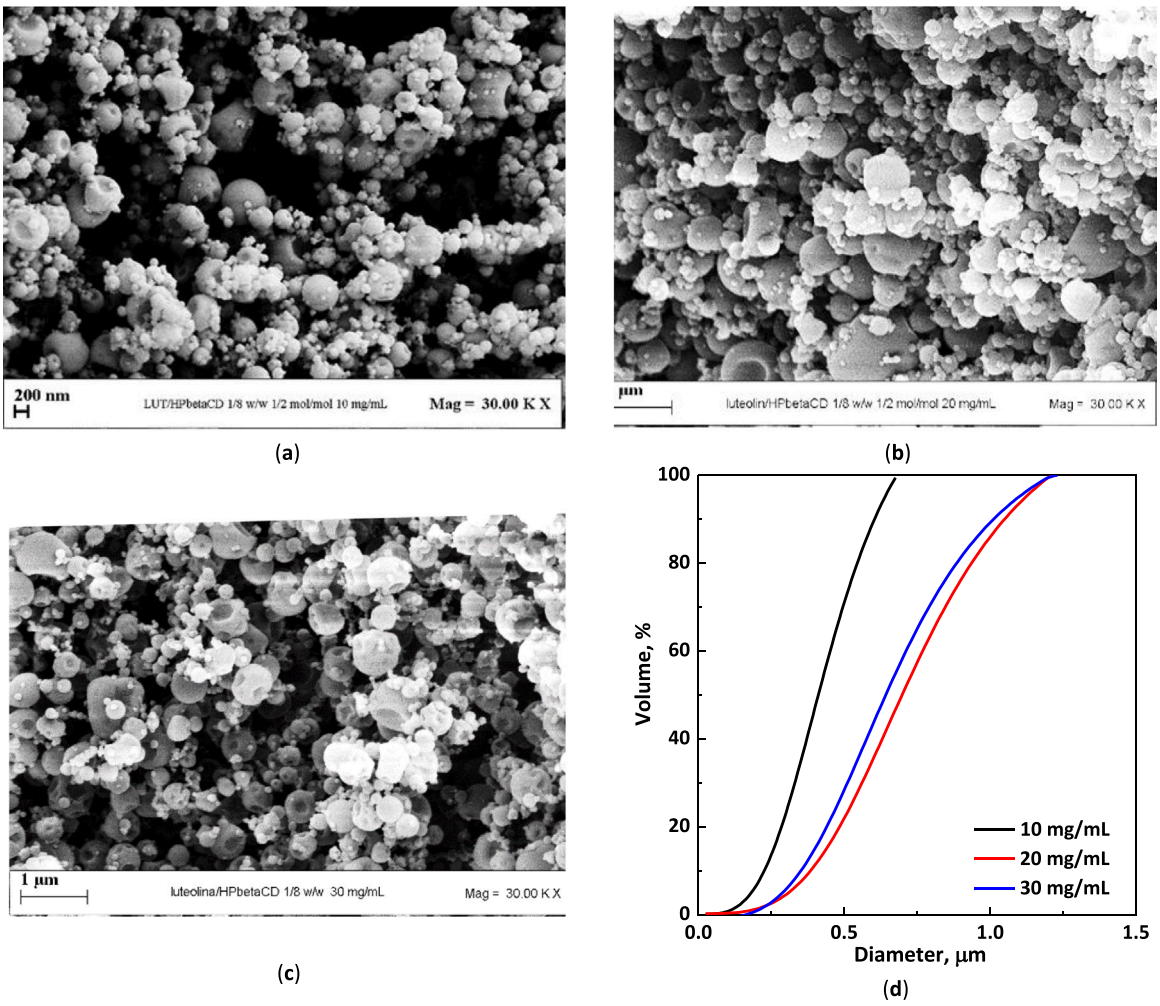

Fig. 4. FESEM images and PSDs of HP-β-CD/LUT particles produced by SAA from EtOH/H_2O 70/30 at 8/1 *w/w*. Effect of the total concentration of the liquid solution: (a) 10 mg/mL; (b) 20 mg/mL; (c) 30 mg/mL; (d) PSDs.

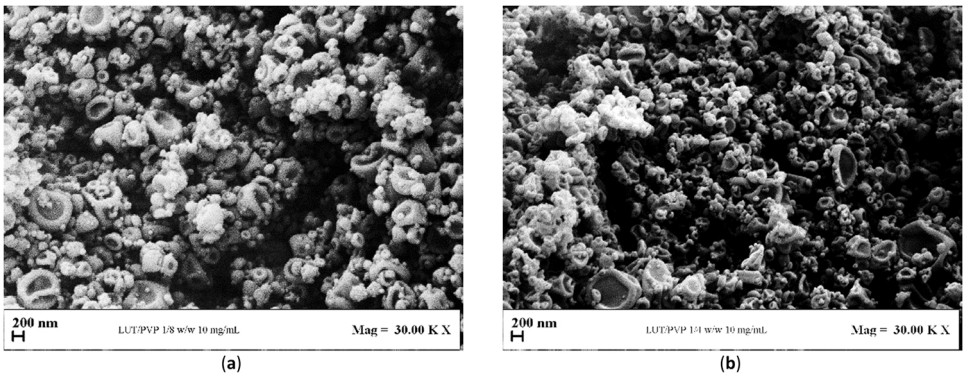

Fig. 5. FESEM images of SAA processed PVP/LUT particles using EtOH/H_2O 70/30 *v/v* at 10 mg/mL. Effect of the PVP/LUT ratio: (a) 8/1 *w/w*; (b) 4/1 *w/w*.

can be observed in the FESEM image reported in Fig. 5b.

Comparing the HP-β-CD/LUT with the PVP/LUT powders, it can be concluded that the former, morphologically, are better as spherical, distinct, and regular particles are obtained, contrary to what happens for powders processed using PVP; in the latter case, holes and cavities are present. Similar results have been obtained previously with different solutes and have been explained with the start of a crystallization process that superimposed to droplet drying [36,37].

3.2. Rutin

3.2.1. HP-β-CD/Rutin

For this system, the HP-β-CD/RUT ratio was fixed at 4/1 w/w, and the total concentration of the liquid solution was varied from 10 to 20 mg/mL. At 10 mg/mL, sub-micrometric spherical particles with an average diameter equal to 0.42 μm were obtained, whereas, at 20 mg/mL, slightly collapsed sub-micrometric particles were precipitated. The concentration was not further increased because of the insolubility of

the HP-β-CD/RUT system in the water/ethanol mixture at concentrations greater than 20 mg/mL. The FESEM images (taken at the same enlargement) of the powders obtained at 10 and 20 mg/mL are reported in Fig. 6. A comparison of the PSDs revealed that the concentration does not influence the particle size because the two curves were very similar.

3.2.2. PVP/Rutin

A test was carried out for the system PVP/RUT at a 10 mg/mL concentration and a polymer/antioxidant ratio equal to 4/1 *w/w*. For this system, no powder was recovered on the filter, and an esigue amount of material was sampled from the walls of the precipitation chamber. Therefore, this system is inefficient in terms of recovery and was not further studied.

3.3. Naringenin

3.3.1. HP-β-CD/Naringenin

In the case of the system HP-β-CD/NAR, the effect of the carrier/active principle ratio and the total concentration on the obtained morphology, mean size, and particle size distribution was evaluated.

First, the concentration of the liquid solution was fixed at 20 mg/mL, and the precipitation was attempted using 9/1 and 4.5/1 w/w ratios. Well-defined particles were obtained in both cases, as evident from the FESEM images reported in Fig. 7.

To maximize the amount of active principle in the obtained formulation, the ratio of 4.5/1 *w/w* was chosen for the following set of experiments at different concentrations. Therefore, the concentration of the liquid solution was varied from 10 to 30 mg/mL. Sub-microparticles were obtained in correspondence of all the concentrations, as can be seen from the FESEM images reported in Fig. 8: it is clear that the particles attained at 10 and 20 mg/mL were spherical and well defined (Figs. 8a and 8b), whereas the powder obtained using a concentration equal to 30 mg/mL are coalescent (Fig. 8c). Increasing the concentration, the mean size increased and the particle size distribution enlarged, as can be seen from the comparison of the FESEM images taken at the same magnification and as is clear from the cumulative volumetric distribution reported in Fig. 8d. Considering that for the HP-β-CD/NAR system, the particle size distributions have a higher standard deviation, in Figs. 8a-8c, the distributions in terms of number of particles are shown in boxes at the top right of the FESEM images, in order to take into account the presence of the smaller particles that could be not evident from the distributions in terms of volume.

3.3.2. PVP/Naringenin

The behavior of the PVP/NAR system was studied by setting a polymer/API ratio of 9/1 *w/w* and working with a total concentration of solutes in the solution equal to 10 mg/mL. Under these conditions, powders of slightly coalescing sub-micrometric dimensions were obtained.

3.4. Characterization

Fourier transform spectroscopic analysis (FT-IR) was achieved to investigate the bands representative of the main functional groups of APIs and carriers, the probable interactions between the API and the carrier, as well as the characteristic bands of both the compounds in the SAA powders.

Regarding the carriers used:

- The spectrum of unprocessed HP-β-CD shows two main absorption bands at 3414 cm^{-1} and 2929 cm^{-1} due to the -OH and CH groups stretchings, a peak at 1638 cm^{-1} attributable to the H–O–H group bending, a peak at 1157 cm^{-1} related to the C–O–C glycosidic bridge asymmetric stretching, and two peaks at 1082 and 1032 cm^{-1} due to the C–C and C–O groups stretchings [33].
- The spectrum of unprocessed PVP shows a characteristic absorption band at 3469 cm^{-1} due to the -OH group stretching, a peak at 1653 cm^{-1} corresponding to the C═O groups stretching, and a peak at 2875 cm^{-1} attributable to the C–H group stretching [30].

In Fig. 9, the spectra of the three APIs when processed with HP-β-CD are reported. In particular, Fig. 9a shows the FTIR spectra relating to pristine luteolin and HP-β-CD, to the HP-β-CD/LUT physical mixture and to the SAA inclusion complexes obtained at different CD/LUT ratios. The spectrum of untreated LUT shows a broad absorption band at 3420 cm^{-1} attributable to the hydroxyl group stretching, a characteristic peak at 1656 cm^{-1} relative to the carbonyl group (C═O) stretching, a peak at 1613 cm^{-1} due to the double bond C═C, two peaks at 1369 cm^{-1} and 1266 cm^{-1} linked to the bending of phenolic hydroxyl groups and a peak at a wavenumber of 1166 cm^{-1} attributable to the C–O–C group stretching [18,30,38]. The characteristic bands of cyclodextrin dominate the spectra of SAA powders; in particular, some distinctive bands of luteolin (blue vertical lines) are visible in the spectrum of the physical mixture but they are absent in the spectrum related to SAA powders. The reduction in intensity or even the partial or total disappearance of bands which are typical of the active compound spectrum indicates the formation of an inclusion complex, as the guest molecule (luteolin) is incorporated into the cavity of the host molecule (CD) and, therefore, its characteristic bands are hidden [34]. The presence of a few characteristic bands of luteolin in SAA coprecipitated powders (green lines) suggests, in particular, the formation of partial complexes, i.e., a small part of the luteolin is located outside the cavity, recording some characteristic peaks. In the case of the SAA processed powders, it is also evident the appearance of a new peak at about 1297 cm^{-1} (orange line), not present both in the spectra of pure LUT and CD and in the physical mixture. The appearance of this band could be attributable to the

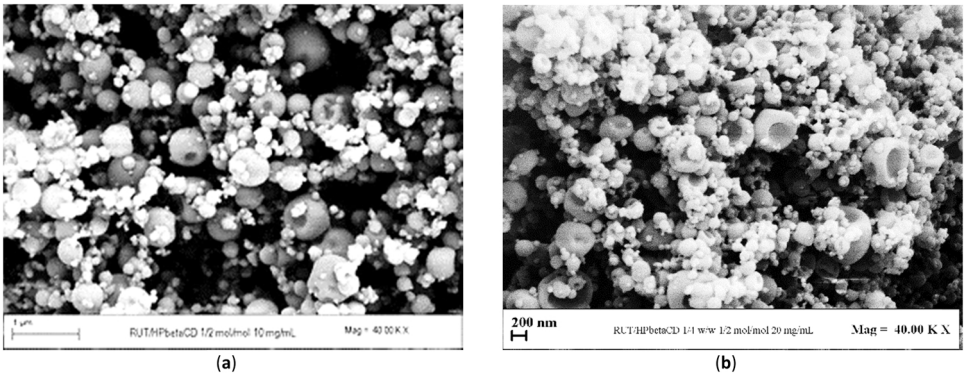

(a) (b)

Fig. 6. FESEM images of HP-β-CD/RUT particles produced by SAA from EtOH/H_2O 70/30 *v/v* at 4/1 *w/w*. Effect of the total concentration: (a) 10 mg/mL; (b) 20 mg/mL.

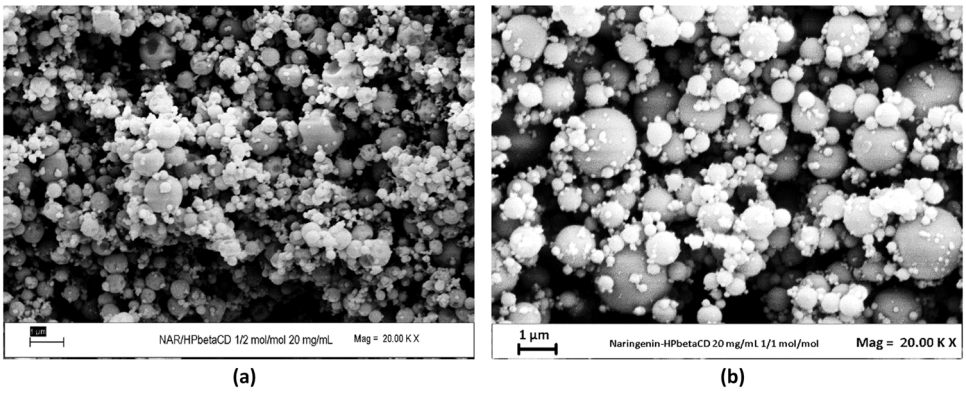

Fig. 7. FESEM images of HP-β-CD/NAR particles produced by SAA from EtOH/H_2O 70/30 *v/v* at 20 mg/mL. Effect of the carrier/NAR ratio: (a) 9/1 *w/w*; (b) 4.5/1 *w/w*.

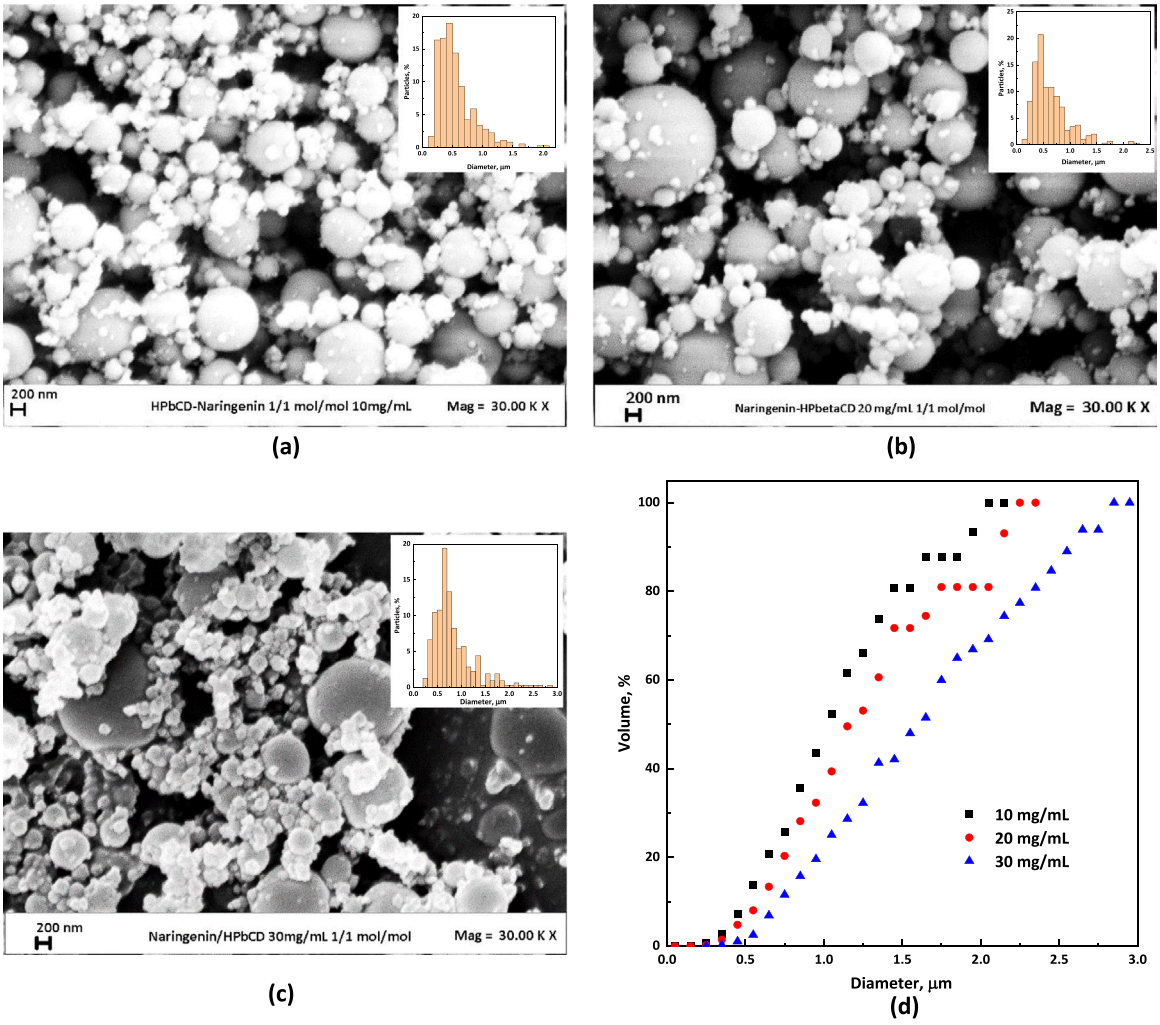

Fig. 8. FESEM images and PSDs of SAA HP-β-CD/NAR particles using EtOH/H_2O 70/30 *v/v* at 4.5/1 *w/w*. Effect of the total concentration of the liquid solution: (a) 10 mg/mL; (b) 20 mg/mL; (c) 30 mg/mL; (d) PSDs.

formation of an inclusion complex.

The FTIR spectra of the samples obtained processing LUT with PVP are reported in Fig. S1 of the Supplementary Material section.

Fig. 9b shows the infrared spectra relating to rutin and HP-β-CD, to their physical mixture, and to the SAA powders obtained with a carrier/drug ratio of 4/1 w/w. It is recalled that the PVP/rutin was excluded from the study as it was not satisfactory in terms of recovery of the powder produced. The spectrum of unprocessed rutin is characterized by a shoulder at 3424 cm^{-1} due to the -OH group stretching [39], an absorption peak at 1654–1600 cm^{-1} attributable to the carbonyl group C═O stretching, and a peak at a wave number equal to 1504 cm^{-1} associated with the aromatic C═C double bond; the bands at 1362–1294 cm^{-1} are attributable instead to the C–O group, while those at 1204–1043 cm^{-1} to the C–O–C groups [34,40]. The reduction in

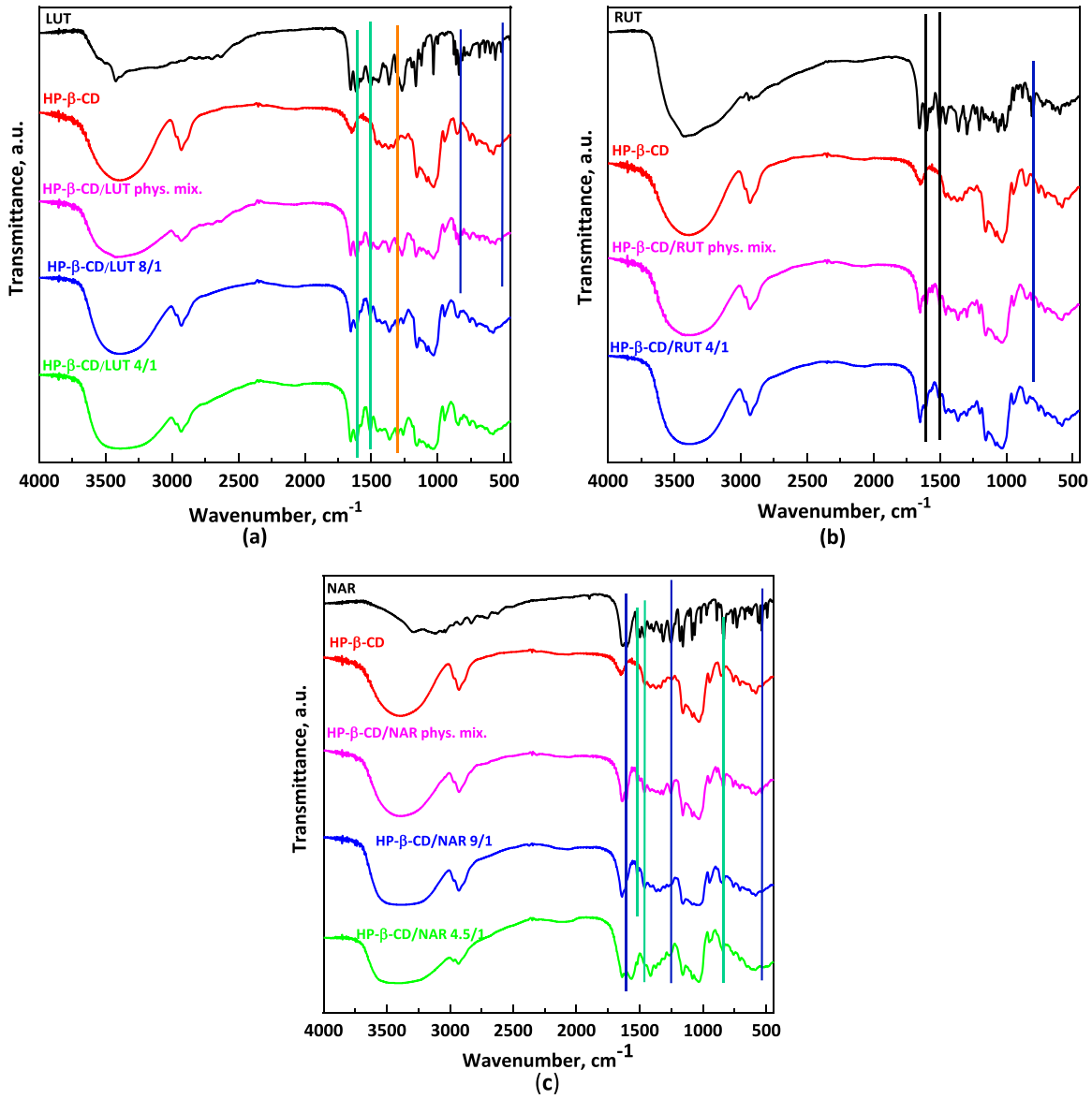

Fig. 9. FT-IR spectra of unprocessed materials, HP-β-CD/API physical mixtures and SAA processed HP-β-CD/API powders: (**a**) LUT; (**b**) RUT; (**c**) NAR. Blue lines: peaks characteristic of the API present in physical mixtures spectra but not in SAA powder ones; green lines: peaks characteritic of the API present in SAA powder spectra; black lines: peacks characteristic of the API present (with reduced intensity) in SAA powder spectra; orange lines: peaks not present in API spectra but present in SAA powder one.

intensity (black vertical lines) or the disappearance (blue vertical line) of some characteristic bands of rutin in the spectrum of SAA powders indicate the probable complexation between CD and rutin, which seems to be at least partially incorporated in the cyclodextrin cavity [34]. It is reasonable to hypothesize a partial complexation in the case of rutin due to its molecular size which is greater than that of the other two flavonoids.

Fig. 9c shows the infrared spectra of naringenin and HP-β-CD, of the HP-β-CD/NAR physical mixture and of SAA powders obtained at different carrier/drug ratios. Pure NAR spectrum shows the characteristic bands of the C═O carbonyl stretching at 1630 cm^{-1} and 1603 cm^{-1}; the band at 1462 cm^{-1} is instead representative of the stretching of the aromatic C═C double bond or of the bending of the C-C-H group. The shoulder at 3290 cm^{-1} is attributable to the -OH group stretching, while the strong band at 832 cm^{-1} corresponds to the *para*-disubstituted benzene present in the naringenin structure [41]. Several characteristic bands of naringenin are visible in the physical mixture (blue lines) but not in the SAA powders, whose spectrum is more similar to that of pure cyclodextrin. Some characteristic bands (green lines) of NAR are visible in the spectrum of SAA powders, indicating that a part of the active principle is located outside the cyclodextrin cavity.

The FTIR spectra of the samples obtained processing NAR with PVP are reported in Fig. S2 of the Supplementary Material section.

In Fig. 10, DSC thermograms of unprocessed antioxidants, PVP, HP-β-CD and SAA coprecipitated powders are reported for LUT (Fig. 10a), RUT (Fig. 10b), and NAR (Fig. 10c). Unprocessed PVP and unprocessed HP-β-CD show broad endothermic events due to the water loss (between 50 and 130 °C in the case of PVP, and between 40 and 100 °C in the case of HP-β-CD). The thermograms of unprocessed flavonoids show and endothermic peak due to the melting point at 340 °C, 174 °C and 252 °C for LUT, RUT and NAR, respectively [40,42,43]. The characteristic peaks of LUT, RUT and NAR are not present in thermograms of SAA processed coprecipitated powders, suggesting that the active principles entrapped inside PVP microparticles and HP-β-CD cavity are in amorphous state. The disappearance of the flavonoid melting peak in the thermograms of the SAA powders also indicated that the complexation

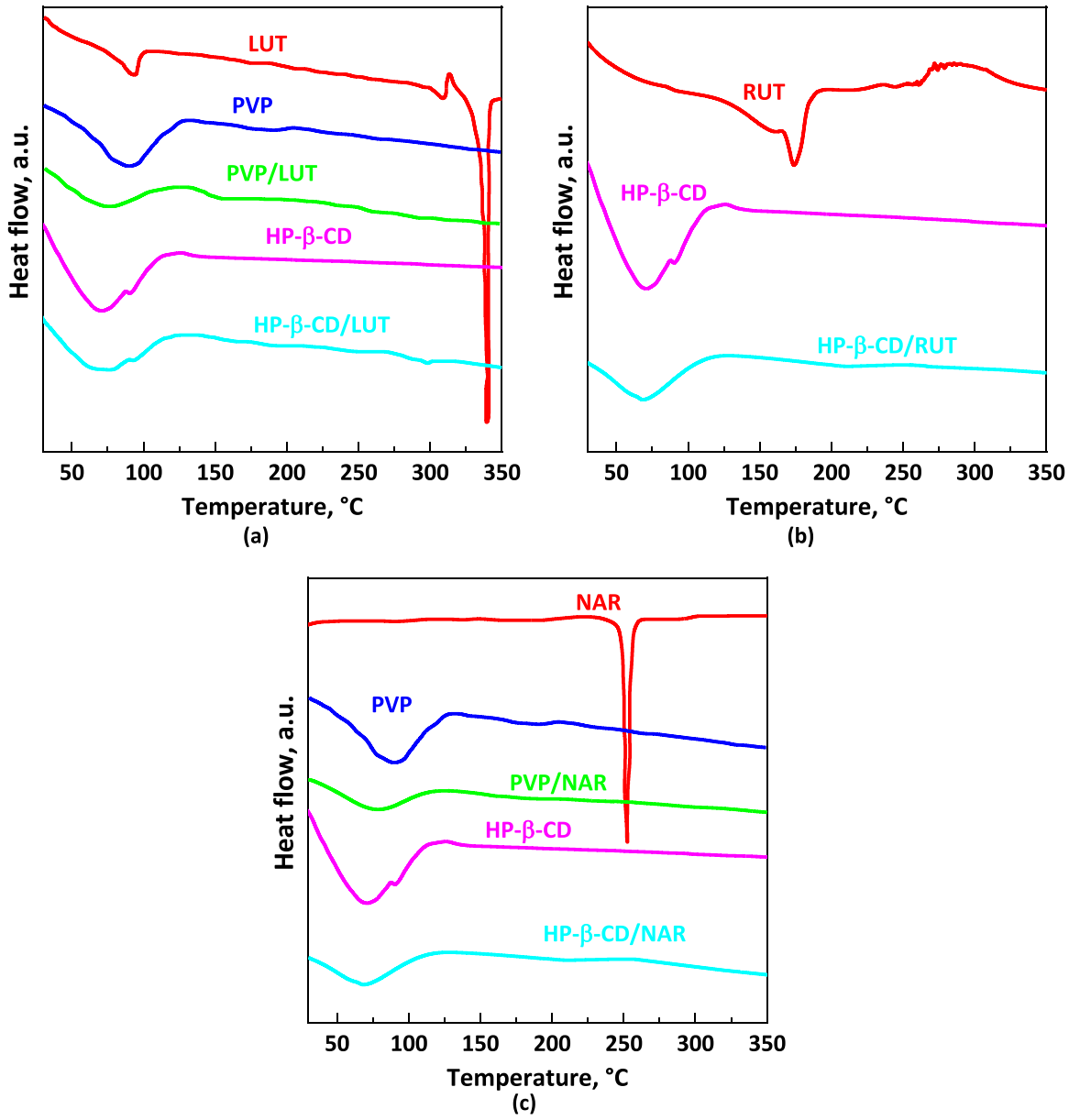

Fig. 10. DSC thermograms of pure materials and SAA processed coprecipitated powders: (a) LUT; (b) RUT; (c) NAR.

occurred; i.e., the active principle is hidden into the cavity of the amorphous HP-β-CD [44–46].

XRD analyses were performed to confirm the amorphous nature of the SAA processed coprecipitated powders and the results are reported in Fig. 11. Unprocessed active principles have crystalline structures, whereas PVP and HP-β-CD patterns clearly indicate their amorphous structure. The patterns related to the SAA coprecipitated powders confirmed the achievement of the amorphization both using PVP and HP-β-CD as the carriers. The characteristic peaks of the active principles disappeared in the XRD patterns of SAA complexes, since the flavonoids were incorporated and hidden in the cavity of the amorphous CDs. Therefore, XRD patterns suggest that inclusion complex formed.

The dissolution profiles were measured to compare the profiles of the pristine active ingredient with the ones of the API released from the particles produced by SAA; in this way, it will be possible to evaluate the effect of the presence of the carrier on the dissolution of the active compound, and to compare the cyclodextrin-based inclusion complexes and the PVP-based coprecipitates.

From Fig. 12a, it is possible to observe that the time necessary to completely dissolve LUT in PBS is very long (the antioxidant dissolves completely after about 62 h). SAA micronized LUT takes 40 h to dissolve; the reduction in dissolution time can be attributed to the smaller diameters of the micronized LUT compared to the unprocessed one. In the case of the physical mixtures obtained mixing LUT with PVP or with HP-β-CD, the time necessary to reach the plateau is equal to 26.7 h and 14.8 h, respectively. The SAA coprecipitated samples, on the other hand, show a much higher dissolution rate, considering both the carriers. When PVP is used as the carrier, LUT contained in the powders produced with a ratio of 4/1 *w/w* dissolves completely in about 9 h, compared to the 4 h required when the ratio is equal to 8/1 *w/w*. For short times, however, the two curves are practically superimposable, releasing about 40% of the active ingredient in 60 min. When LUT is processed using a HP-β-CD/LUT ratio equal to 8/1 *w/w*, the complete dissolution occurs in about 2 h; the time is halved when using a ratio of 4/1 *w/w*. In fact, in the latter case it can be observed that 95% of the active ingredient is released in just under half an hour; at the same time, the sample with a higher ratio releases just 30% of the active principle. This trend may seem unusual when compared with the results obtained

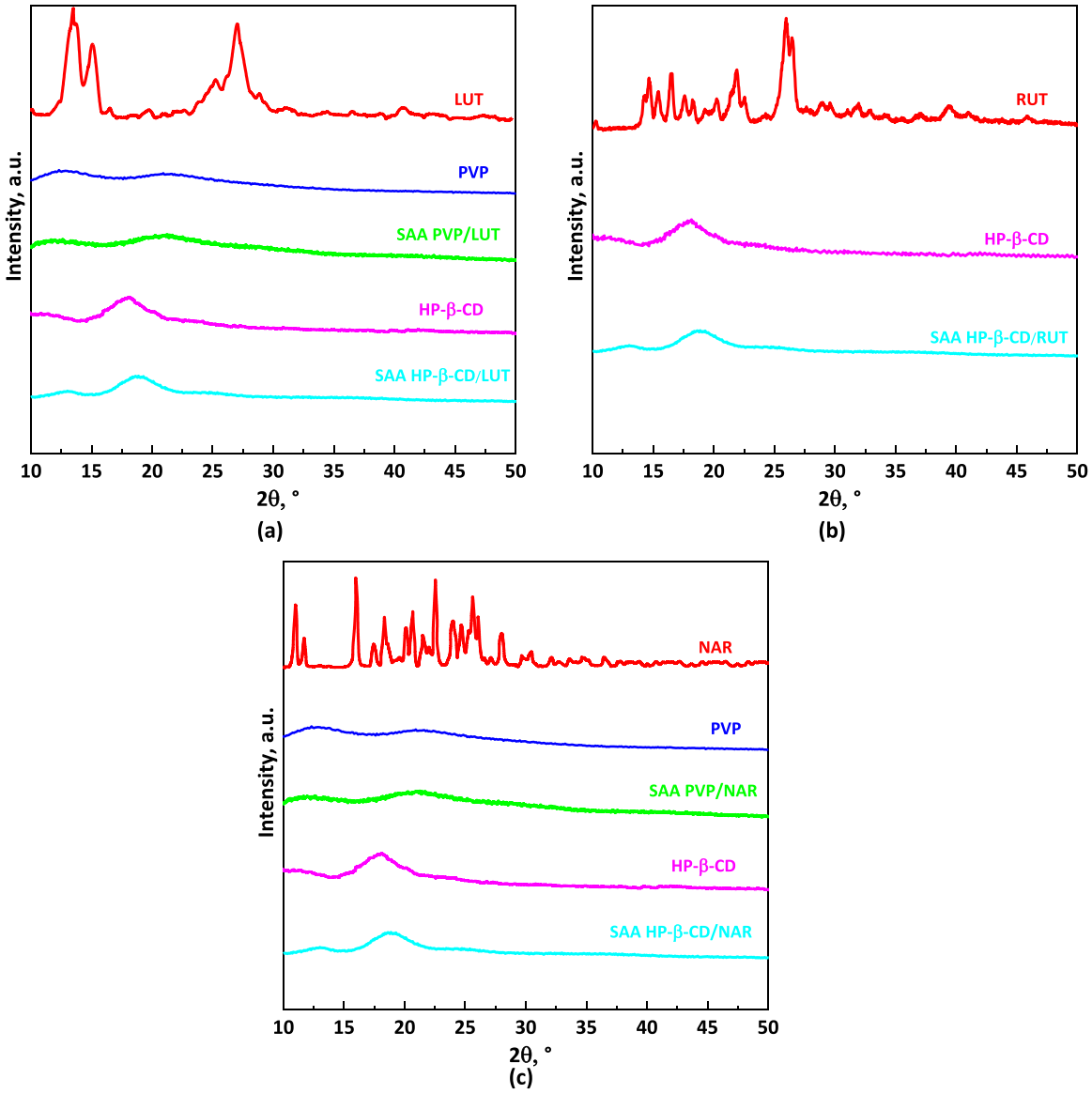

Fig. 11. XRD patterns of pure materials and SAA processed coprecipitated powders: (a) LUT; (b) RUT; (c) NAR.

in previous works focused on the production of composite particles using other polymeric carriers [29], in which higher quantities of carriers corresponded to an increase in the dissolution rate of the drug incorporated in the polymer particles. However, the trend obtained in the case of HP-β-CD/LUT inclusion complexes has already been observed in some previous studies [18,30,47], where the result obtained is attributed to the formation of weak intermolecular interactions between the active compound and carriers, which positively affect the dissolution rate. It is known that the formation of cyclodextrin/active ingredient complexes actually involves the formation of weak Van der Waals-type interactions or hydrogen bridges. This result can therefore be considered as a demonstration of the formation of HP-β-CD/LUT inclusion complexes even at low carrier/API weight ratios. Comparing the release profiles obtained using the two carriers, it appears evident that HP-β-CD is more effective than PVP in increasing the dissolution rate of luteolin. Both curves relating to PVP/LUT coprecipitates show, in fact, longer dissolution times of the active principle compared to the HP-β-CD/LUT complexes. Even in the latter case, using smaller quantities of carriers, i.e. for carrier/LUT ratio equal to 4/1 *w/w*, the dissolution kinetics are faster, releasing 90% of the active ingredient in about half an hour. The corresponding PVP/LUT coprecipitated powder would take 10.5 times longer.

As regards the HP-β-CD/RUT system, the results of the release tests in PBS at pH 7.4 are shown in Fig. 12b. The improvement in dissolution rates is due to the SAA micronization and to the presence of HP-β-CD (also in the case of the physical mixture the time required to dissolve the API is shorter than the dissolution time of RUT as it is). Unprocessed rutin takes more than 73 h to completely dissolve; in the case of SAA powders obtained by setting a weight ratio equal to 8/1, less than 23 h are sufficient. It is also interesting to note that in the latter case, 90% of the active ingredient is released in just 7.9 h, a time 3.8 times shorter than that required for rutin as it is. It should be remembered that it was not possible to carry out dissolution tests for the PVP/RUT system as, as reported in the previous section, the SAA technique does not seem to be suitable for the precipitation of RUT and PVP since it was not possible to recover powder downstream of the test. In the case of rutin, therefore, cyclodextrin appears to be the appropriate carrier primarily in terms of recovery/production of composite powders.

Finally, in Fig. 12c, a comparison between the dissolution profiles of pure NAR, of the physical mixtures obtained using HP-β-CD and PVP as the carriers, and of the SAA samples obtained by setting a carrier/NAR ratio equal to 9/1 and 4.5/1 *w/w* is reported. It is possible to observe

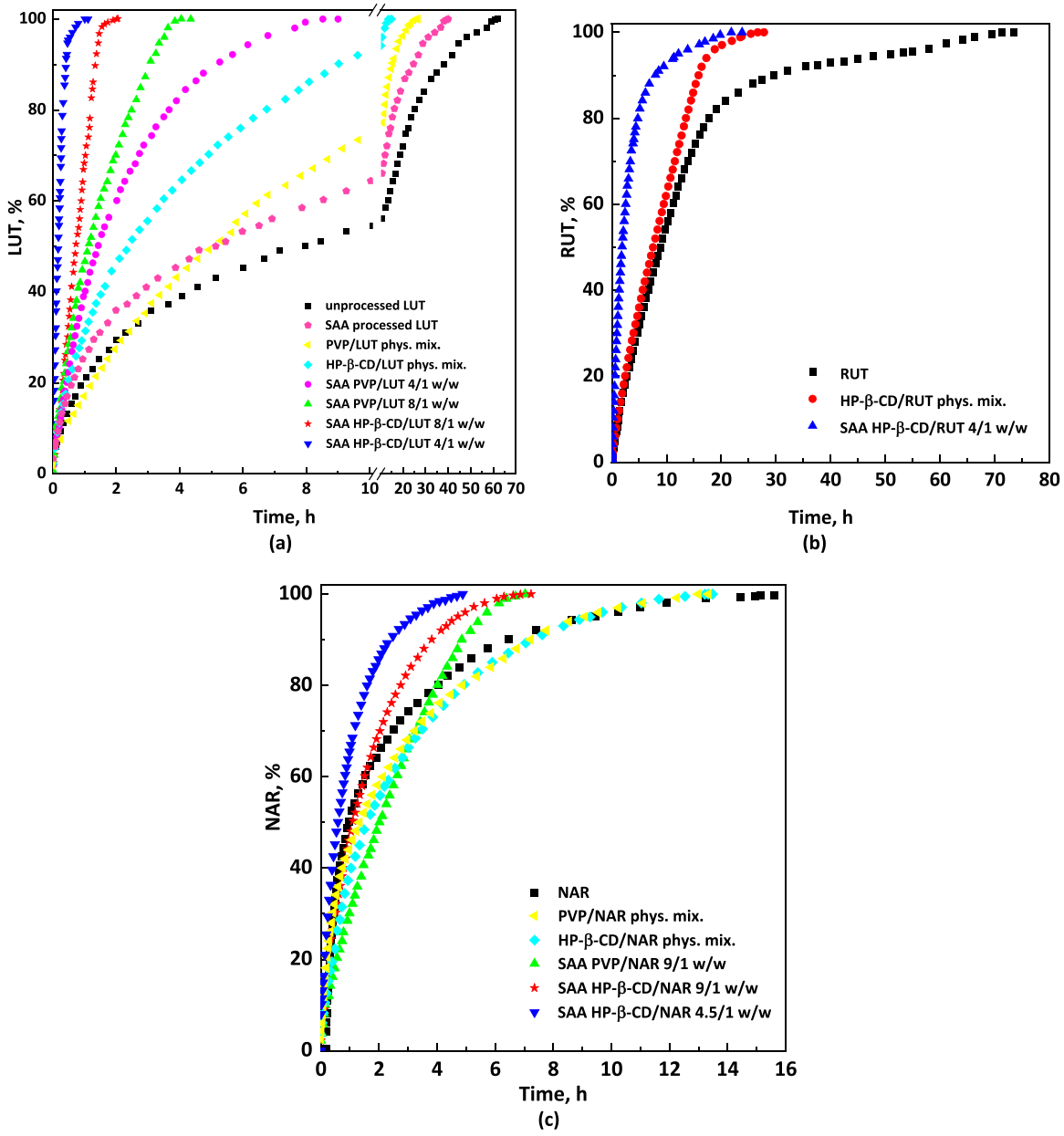

Fig. 12. Dissolution profiles of flavonoids in PBS from powders coprecipitated with PVP and HP-β-CD: (a) LUT; (b) RUT; (c) NAR.

that naringenin as it is dissolved completely in 16.4 h and both physical mixtures show dissolution kinetics similar to the unprocessed API. In the case of PVP/NAR coprecipitated powders, the dissolution of NAR was accelerated for only 20% of the drug present in the SAA powders. This result indicates an ineffective co-precipitation of naringenin with PVP, as most of the naringenin is either not trapped in the polymer matrix or is located above/near the surface of the particle. Therefore, the carrier's presence does not greatly affect the dissolution of the API. The quantity of naringenin actually incorporated in the cyclodextrin cavity appears to be higher, since 40% of the active ingredient is released more rapidly by HP-β-CD than unprocessed naringenin. This result suggests the partial complexation between naringenin and cyclodextrin. In any case, for the HP-β-CD/NAR, the active compound is released in 7.23 h when 9/1 *w/w* is used; so the dissolution of naringenin was speeded up by 2.3 times, compared to pure NAR. Decreasing the carrier/NAR ratio to 4.5/1 *w/w*, the dissolution rate increases. Indeed, the API is completely dissolved in 4.88 h, which means that, compared to the drug as it is, the dissolution is 3.4 times faster.

4. Conclusions

In this work, the applicability of the SAA process in obtaining inclusion complexes or coprecipitated sub-microparticles containing antioxidant compounds (luteolin, rutin or naringenin) promising for the treatment of the CoVID-19 pathology was tested. In order to improve the bioavailability of these poorly soluble compounds in water, two different carriers were selected, HP-β-CD and PVP. It emerged that the use of HP-β-CD allows the formation of more defined and regular particles than PVP for all three active ingredients examined.

The dissolution tests showed much shorter release times of the antioxidants from the SAA powders than the pure active compounds for all the systems analyzed. In particular, HP-β-CD was found to be a more effective carrier than PVP in improving the dissolution rate of the three APIs, as it allowed these compounds to be dissolved faster and using smaller quantities of carrier. In particular, in the case of rutin, the choice of cyclodextrin is necessary for an effective production in terms of powder recovery.

It can therefore be concluded that the SAA process is effective for the formation of inclusion complexes containing luteolin, rutin or naringenin, improving their dissolution more efficiently than simple coprecipitation with PVP.

Declaration of Competing Interest

The author declares that she has no known competing financial interests or personal relationships that could have appeared to influence the work reported in this paper.

Acknowledgments

The author is grateful to Federica Casillo for her help in performing part of the experiments during her Master's Thesis in Chemical Engineering at the Department of Industrial Engineering of the University of Salerno.

Appendix A. Supporting information

Supplementary data associated with this article can be found in the online version at doi:10.1016/j.supflu.2022.105604.

References

[1] T. Singhal, A review of coronavirus disease-2019 (COVID-19), Indian J. Pediatr. 87 (2020) 281–286, https://doi.org/10.1007/s12098-020-03263-6.
[2] N. Muralidharan, R. Sakthivel, D. Velmurugan, M.M. Gromiha, Computational studies of drug repurposing and synergism of lopinavir, oseltamivir and ritonavir binding with SARS-CoV-2 protease against COVID-19, J. Biomol. Struct. Dyn. 39 (2021) 2673–2678, https://doi.org/10.1080/07391102.2020.1752802.
[3] B. Cao, Y. Wang, D. Wen, W. Liu, J. Wang, et al., A trial of lopinavir-ritonavir in adults hospitalized with severe covid-19, N. Eng. J. Med. 382 (2020) 1787–1799, https://doi.org/10.1056/NEJMoa2001282.
[4] Y. Wang, D. Zhang, G. Du, R. Du, J. Zhao, et al., Remdesivir in adults with severe COVID-19: a randomised, double-blind, placebo-controlled, multicentre trial, Lancet 395 (2020) 1569–1578, https://doi.org/10.1016/S0140-6736(20)31022-9.
[5] A.A. Elfiky, Ribavirin, Remdesivir, Sofosbuvir, Galidesivir, and Tenofovir against SARS-CoV-2 RNA dependent RNA polymerase (RdRp): a molecular docking study, Life Sci. 253 (2020), https://doi.org/10.1016/j.lfs.2020.117592.
[6] B. Morgenstern, M. Michaelis, P.C. Baer, H.W. Doerr, J. Cinatl Jr., Ribavirin and interferon-β synergistically inhibit SARS-associated coronavirus replication in animal and human cell lines, Biochem. Biophys. Res. Commun. 326 (2005) 905–908, https://doi.org/10.1016/j.bbrc.2004.11.128.
[7] D. Vlachakis, E. Papakonstantinou, T. Mitsis, K. Pierouli, I. Diakou, G. Chrousos, F. Bacopoulou, Molecular mechanisms of the novel coronavirus SARS-CoV-2 and potential anti-COVID19 pharmacological targets since the outbreak of the pandemic, Food Chem. Toxicol. 146 (2020), https://doi.org/10.1016/j.fct.2020.111805.
[8] A.D.S. Antonio, L.S.M. Wiedemann, V.F. Veiga-Junior, Natural products' role against COVID-19, RSC Adv. 10 (2020) 23379–23393, https://doi.org/10.1039/d0ra03774e.
[9] M. Lotfi, M.R. Hamblin, N. Rezaei, COVID-19: transmission, prevention, and potential therapeutic opportunities, Clin. Chim. Acta 508 (2020) 254–266, https://doi.org/10.1016/j.cca.2020.05.044.
[10] F. Batool, E.U. Mughal, K. Zia, A. Sadiq, N. Naeem, A. Javid, Z. Ul-Haq, M. Saeed, Synthetic flavonoids as potential antiviral agents against SARS-CoV-2 main protease, J. Biomol. Struct. Dyn. (2020), https://doi.org/10.1080/07391102.2020.1850359.
[11] S. Kumar, A.K. Pandey, Chemistry and biological activities of flavonoids: an overview, Sci. World J. (2013)) (2013), https://doi.org/10.1155/2013/162750.
[12] R. Patil, R. Chikhale, P. Khanal, N. Gurav, M. Ayyanar, et al., Computational and network pharmacology analysis of bioflavonoids as possible natural antiviral compounds in COVID-19, Inform. Med. Unlocked 22 (2021), https://doi.org/10.1016/j.imu.2020.100504.
[13] A. Filippini, A. D'Amore, F. Palombi, A. Carpaneto, Could the inhibition of endo-lysosomal two-pore channels (TPCs) by the natural flavonoid naringenin represent an option to fight SARS-CoV-2 infection? Front. Microbiol. 11 (2020) 970, https://doi.org/10.3389/fmicb.2020.00970.
[14] H. Tutunchi, F. Naeini, A. Ostadrahimi, M.J. Hosseinzadeh-Attar, Naringenin, a flavanone with antiviral and anti-inflammatory effects: a promising treatment strategy against COVID-19, Phytother. Res. 34 (2020) 3137–3147, https://doi.org/10.1002/ptr.6781.
[15] N.M. Abd El-Aziz, O.M. Eldin Awad, M.G. Shehata, S.A. El-Sohaimy, Inhibition of the SARS-CoV-2 RNA-Dependent RNA polymerase by natural bioactive compounds: molecular docking analysis, Egypt. J. Chem. 64 (2021) 1989–2001, https://doi.org/10.21608/EJCHEM.2021.45739.2947.
[16] Y. Yang, M.S. Islam, J. Wang, Y. Li, X. Chen, Traditional Chinese medicine in the treatment of patients infected with 2019-new coronavirus (SARS-CoV-2): a review and perspective, Int. J. Biol. Sci. 16 (2020) 1708, https://doi.org/10.7150/ijbs.45538.
[17] W. Ngwa, R. Kumar, D. Thompson, W. Lyerly, R. Moore, T.E. Reid, H. Lowe, N. Toyang, Potential of flavonoid-inspired phytomedicines against COVID-19, Molecules 25 (2020), https://doi.org/10.3390/molecules25112707.
[18] A. Di Capua, R. Adami, L. Izzo, E. Reverchon, Luteolin/dextran-FITC fluorescent microspheres produced by supercritical assisted atomization, J. Supercrit. Fluids 130 (2017) 97–104, https://doi.org/10.1016/j.supflu.2017.07.034.
[19] V. Prosapio, I. De Marco, E. Reverchon, Supercritical antisolvent coprecipitation mechanisms, J. Supercrit. Fluids 138 (2018) 247–258, https://doi.org/10.1016/j.supflu.2018.04.021.
[20] P. Franco, I.De Marco, Supercritical antisolvent process for pharmaceutical applications: a review, Processes 8 (2020) 938, https://doi.org/10.3390/pr8080938.
[21] L. MacEachern, A. Kermanshahi-Pour, M. Mirmehrabi, Supercritical carbon dioxide for pharmaceutical co-crystal production, Cryst. Growth Des. 20 (2020) 6226–6244, https://doi.org/10.1021/acs.cgd.0c00571.
[22] L. Baldino, S. Cardea, E. Reverchon, Supercritical assisted electrospray: an improved micronization process, Polymers 11 (2019), https://doi.org/10.3390/polym11020244.
[23] K. Tutek, A. Masek, A. Kosmalska, S. Cichosz, Application of fluids in supercritical conditions in the polymer industry, Polymers 13 (2021) 1–17, https://doi.org/10.3390/polym13050729.
[24] P. Trucillo, R. Campardelli, M. Scognamiglio, E. Reverchon, Control of liposomes diameter at micrometric and nanometric level using a supercritical assisted technique, J. CO2 Util. 32 (2019) 119–127, https://doi.org/10.1016/j.jcou.2019.04.014.
[25] R.L. Matos, T. Lu, V. Prosapio, C. McConville, G. Leeke, A. Ingram, Coprecipitation of curcumin/PVP with enhanced dissolution properties by the supercritical antisolvent process, J. CO2 Util. 30 (2019) 48–62, https://doi.org/10.1016/j.jcou.2019.01.005.
[26] S. Taki, E. Badens, G. Charbit, Controlled release system formed by supercritical anti-solvent coprecipitation of a herbicide and a biodegradable polymer, J. Supercrit. Fluids 21 (2001) 61–70, https://doi.org/10.1016/S0896-8446(01)00076-6.
[27] I. De Marco, P. Franco, Effect of the carrier on the coprecipitation of curcumin through supercritical-assisted atomization, ChemEngineering 5 (2021), https://doi.org/10.3390/chemengineering5030059.
[28] R. Adami, S. Liparoti, G. Della Porta, P. Del Gaudio, E. Reverchon, Lincomycin hydrochloride loaded albumin microspheres for controlled drug release, produced by Supercritical Assisted Atomization, J. Supercrit. Fluids 119 (2017) 203–210, https://doi.org/10.1016/j.supflu.2016.09.017.
[29] R. Adami, A. Di Capua, E. Reverchon, Supercritical Assisted Atomization for the production of curcumin-biopolymer microspheres, Powder Technol. 305 (2017) 455–461, https://doi.org/10.1016/j.powtec.2016.10.020.
[30] A. Di Capua, R. Adami, E. Reverchon, Production of luteolin/biopolymer microspheres by supercritical assisted atomization, Ind. Eng. Chem. Res. 56 (2017) 4334–4340, https://doi.org/10.1021/acs.iecr.7b00211.
[31] G. Ozkan, P. Franco, E. Capanoglu, I. De Marco, PVP/flavonoid coprecipitation by supercritical antisolvent process, Chem. Eng. Process. 146 (2019) 1–10, https://doi.org/10.1016/j.cep.2019.107689.
[32] K. Karthikeyan, R. Lakra, R. Rajaram, P.S. Korrapati, Development and characterization of zein-based micro carrier system for sustained delivery of aceclofenac sodium, AAPS PharmSciTech 13 (2012) 143–149, https://doi.org/10.1208/s12249-011-9731-x.
[33] H. Yin, C. Wang, J. Yue, Y. Deng, S. Jiao, Y. Zhao, J. Zhou, T. Cao, Optimization and characterization of 1,8-cineole/hydroxypropyl-β-cyclodextrin inclusion complex and study of its release kinetics, Food Hydrocoll. 110 (2021), https://doi.org/10.1016/j.foodhyd.2020.106159.
[34] P. Franco, I. De Marco, Formation of rutin–β-cyclodextrin inclusion complexes by supercritical antisolvent precipitation, Polymers 13 (2021) 1–15, https://doi.org/10.3390/polym13020246.
[35] C. Luo, W. Liang, X. Chen, J. Wang, Z. Deng, H. Zhang, Pharmaceutical cocrystals of naringenin with improved dissolution performance, CrystEngComm 20 (2018) 3025–3033, https://doi.org/10.1039/c8ce00341f.
[36] E. Reverchon, R. Adami, I. De Marco, C. Laudani, A. Spada, Pigment Red 60 micronization using supercritical fluids based techniques, J. Supercrit. Fluids 35 (2005) 76–82, https://doi.org/10.1016/j.supflu.2004.10.010.
[37] R. Adami, S. Liparoti, A. Di Capua, M. Scognamiglio, E. Reverchon, Production of PEA composite microparticles with polyvinylpyrrolidone and luteolin using Supercritical Assisted Atomization, J. Supercrit. Fluids 143 (2019) 82–89, https://doi.org/10.1016/j.supflu.2018.07.020.
[38] H. Dong, X. Yang, J. He, S. Cai, K. Xiao, L. Zhu, Enhanced antioxidant activity, antibacterial activity and hypoglycemic effect of luteolin by complexation with manganese (II) and its inhibition kinetics on xanthine oxidase, RSC Adv. 7 (2017) 53385–53395, https://doi.org/10.1039/C7RA11036G.
[39] S. Zhang, Y. Han, Preparation, characterisation and antioxidant activities of rutin-loaded zein-sodium caseinate nanoparticles, PLoS One 13 (2018), e0194951, https://doi.org/10.1371/journal.pone.0194951.
[40] M.K. Remanan, F. Zhu, Encapsulation of rutin using quinoa and maize starch nanoparticles, Food Chem. 353 (2021), 128534, https://doi.org/10.1016/j.foodchem.2020.128534.
[41] S. Maity, A.S. Chakraborti, Formulation, physico-chemical characterization and antidiabetic potential of naringenin-loaded poly D, L lactide-co-glycolide (N-PLGA)

nanoparticles, Eur. Polym. J. 134 (2020), 109818, https://doi.org/10.1016/j.eurpolymj.2020.109818.
[42] Y. Luo, S. Chen, J. Zhou, J. Chen, L. Tian, et al., Luteolin cocrystals: characterization, evaluation of solubility, oral bioavailability and theoretical calculation, J. Drug Del. Sci. Tech. 50 (2019) 248–254, https://doi.org/10.1016/j.jddst.2019.02.004.
[43] D.K. Jha, D.S. Shah, P.D. Amin, Thermodynamic aspects of the preparation of amorphous solid dispersions of Naringenin with enhanced dissolution rate, Int. J. Pharm. 583 (2020), 119363, https://doi.org/10.1016/j.ijpharm.2020.119363.
[44] S.W. Jun, M.-S. Kim, J.-S. Kim, H.J. Park, S. Lee, J.-S. Woo, S.-J. Hwang, Preparation and characterization of simvastatin/hydroxypropyl-β-cyclodextrin inclusion complex using supercritical antisolvent (SAS) process, Eur. J. Pharm. Biopharm. 66 (2007) 413–421.
[45] Y. Huang, Y. Zu, X. Zhao, M. Wu, Z. Feng, Y. Deng, C. Zu, L. Wang, Preparation of inclusion complex of apigenin-hydroxypropyl-β-cyclodextrin by using supercritical antisolvent process for dissolution and bioavailability enhancement, Int. J. Pharm. 511 (2016) 921–930.
[46] R. Zhou, F. Wang, Z. Guo, Y. Zhao, Preparation and characterization of resveratrol/hydroxypropyl-β-cyclodextrin inclusion complex using supercritical antisolvent technology, J. Food Process Eng. 35 (2012) 677–686.
[47] P. Franco, I. De Marco, Preparation of non-steroidal anti-inflammatory drug/β-cyclodextrin inclusion complexes by supercritical antisolvent process, J. CO2 Util. (2021), https://doi.org/10.1016/j.jcou.2020.101397.